ELSEVIER

Analytica Chimica Acta 466 (2002) 201–212

ANALYTICA CHIMICA ACTA

www.elsevier.com/locate/aca

Characterization of oxidoreductase–redox polymer electrostatic film assembly on gold by surface plasmon resonance spectroscopy and Fourier transform infrared–external reflection spectroscopy

Aleksandr L. Simonian [a,b,*,1], Alexander Revzin [b,1], James R. Wild [a], Jerry Elkind [c], Michael V. Pishko [d,2]

[a] *Department of Biochemistry and Biophysics, Texas A&M University, College Station, TX 77843-2128, USA*
[b] *Department of Chemical Engineering, Texas A&M University, College Station, TX 77843-3122, USA*
[c] *Texas Instruments Inc., 13536 N. Central Expressway, MS 945, Dallas, TX 75243, USA*
[d] *Department of Chemical Engineering, The Pennsylvania State University, 104 Fenske Laboratory, University Park, PA 16802-4400, USA*

Received 5 March 2002; received in revised form 20 June 2002; accepted 1 July 2002

Abstract

The electrostatic assembly of nanocomposite thin films consisting of alternating layers of an organometallic redox polymer (RP) and oxidoreductase enzymes, glucose oxidase (GOX), lactate oxidase (LOX) and pyruvate oxidase (PYX), was investigated. Multilayer nanostructures were fabricated on gold surfaces by the deposition of an anionic self-assembled monolayer of 11-mercaptoundecanoic acid, followed by the electrostatic attachment of a cationic RP, poly(vinylpyridine $Os(bis\text{-}bipyridine)_2Cl$-co-allylamine) (PVP-Os-AA), and anionic oxidoreductase enzymes. Surface plasmon resonance (SPR) spectroscopy, Fourier transform infrared external reflection spectroscopy (FT-IR–ERS) and electrochemistry were employed to characterize the assembly of these nanocomposite films. The surface concentration of GOX was found to be 2.4 ng/mm^2 for the first enzyme layer and 1.96 ng/mm^2 for the second enzyme layer, while values of 10.7 and 1.3 ng/mm^2 were obtained for PYX and LOX, respectively. The apparent affinity constant for GOX adsorption was found to be 8×10^7 M^{-1}. FT-IR–ERS was used to verify the incorporation of GOX and its conformational stability inside of these nanocomposite thin films. An SPR instrument with a flow-through cell was modified by additions of Ag/AgCl reference and Pt counter electrodes, with the gold-coated SPR surface film serving as the working electrode. This enabled real-time observation of the assembly of sensing components and immediate, in situ electrochemical verification of substrate-dependent current upon the addition of enzyme to the multilayer structure. A glucose-dependant amperometric response with sensitivity of 0.197 μA/cm^2/mM for a linear range of 1–10 mM of glucose was obtained. The SPR and FT-IR–ERS studies also showed no desorption of polymer or enzyme from the nanocomposite RP–GOX structure when stored in aqueous environment occurred over the period of 3 weeks, suggesting that decreasing substrate sensitivity with time was due to loss of enzymatic activity rather than loss of film compounds from the nanostructure.

Keywords: Oxidoreductase; Redox polymer; Electrostatic film assembly; Biosensor; Enzyme electrode

* Corresponding author. Tel.: +1-979-845-6840; fax: +1-979-845-9274.
E-mail addresses: als@pop.tamu.edu (A.L. Simonian), mpishko@engr.psu.edu (M.V. Pishko).
[1] Both authors contributed equally to this work.
[2] Co-corresponding author. Tel.: +1-814-863-4810; fax: +1-814-865-7846.

0003-2670/02/$ – see front matter © 2002 Elsevier Science B.V. All rights reserved.
PII: S0003-2670(02)00603-7

1. Introduction

The electrostatic layer-by-layer assembly of nanocomposite films composed of alternating layers of oppositely charged molecules has been a subject of numerous publications [1–4]. A promising application of this assembly approach is in the area of biosensor fabrication. Layer-by-layer assembly represents a potentially reproducible method to control the architecture of the nanometer-scale biosensing films. In addition, electrostatic assembly of sensing layers is well-suited for mediated electrochemical sensing approaches using charged macromolecular electron acceptor/donors and oxidoreductases. First proposed and implemented by Heller [5], this method entails the electrostatic binding between cationic redox polymers (RPs) and anionic oxidoreductase enzymes which results in the transfer of electrons from the enzyme via the redox polymer to the electrode surface [6,7]. Thus, layer-by-layer assembly of oppositely charged redox polymers and oxidoreductase enzymes takes advantage of this method. Biosensors based on various electrostatically complexed redox polymer and enzyme pairs have been successfully used to detect glucose, lactate and other analytes [8–11]. While much attention has been directed to the implementation of the electrostatically assembled biosensors, few studies have sought to characterize the layer-by-layer electrostatic assembly process. Calvo and co-workers [12,13] used QCM, AFM, and electrochemical analysis to investigate the assembly process while others employed XPS and surface plasmon resonance (SPR) for the same purpose [11,14].

In this manuscript, we characterize electrostatically assembled nanocomposite thin films containing redox polymers and oxidoreductases using surface plasmon resonance spectroscopy and Fourier transform infrared–external reflection spectroscopy (FT-IR–ERS). While emphasis in this study was placed on the characterization of the assembly of thin films containing glucose oxidase (GOX), we have also investigated composite structures containing POD and lactate oxidase (LOX) with SPR. Binding interaction SPR curves for all three enzymes were generated and analyzed. Surface concentration and surface coverage for the deposition of GOX, LOX and POD were determined. Affinity constants for the assembly of GOX layer were determined. Incorporation of a GOX and its conformational stability has been examined by FT-IR–ERS. In addition, simultaneous SPR and electrochemical experiments were used to demonstrate enzymatic activity and electron transfer between the redox polymer and enzyme.

2. Materials and methods

2.1. Reagents

Glucose oxidase (GOX, EC 1.1.3.4, Type X-S, 128 units/mg solid from *Aspergillus niger*) and lactate oxidase (LAX, 35 units/mg solid, from *Pediococcus* species) were obtained from the Sigma–Aldrich Chemical Co. Pyruvate oxidase (PYX, EC 1.2.3.3, M_W 260,000) was purchased from Toyobo America Inc. (New York, NY, USA). The 11-mercaptoundecanoic acid (MUA) was obtained from the Aldrich. All reagents, unless otherwise stated, were used as received. Phosphate buffered saline (PBS: 10 mM phosphate, 138 mM NaCl, and 2.7 mM KCl) was in 18 MΩ cm distilled, deionized water (E-pure, Barnstead). Silver epoxy was obtained from Epoxy Technologies (Billerica, MA). Polycationic redox polymer, poly(vinylpyridine Os(bis-bipyridine)$_2$Cl-co-allylamine) (PVP-Os-AA) was synthesized according to the procedures described previously [9,15]. Silicon wafers coated with Cr (20 Å) and Au (500 Å) were purchased from Lance Goddard Associates (Foster City, CA).

3. Equipment and procedures

3.1. SPR analysis of the assembly of nanocomposite films

The Spreeta sensor, a miniature (approximately 7 g), fully integrated surface plasmon resonance device produced by Texas Instruments, was described in detail elsewhere [16,17]. Briefly, the sensor possesses a light-emitting diode with a wavelength of 825 nm, a polarizer, a thermistor, and two 128-pixel silicon photodiode arrays (EOC 1401). A schematic of the device is shown in Fig. 1A. All components are seated on a small printed circuit board and encapsulated with clear, optical epoxy (index of refraction of 1.52),

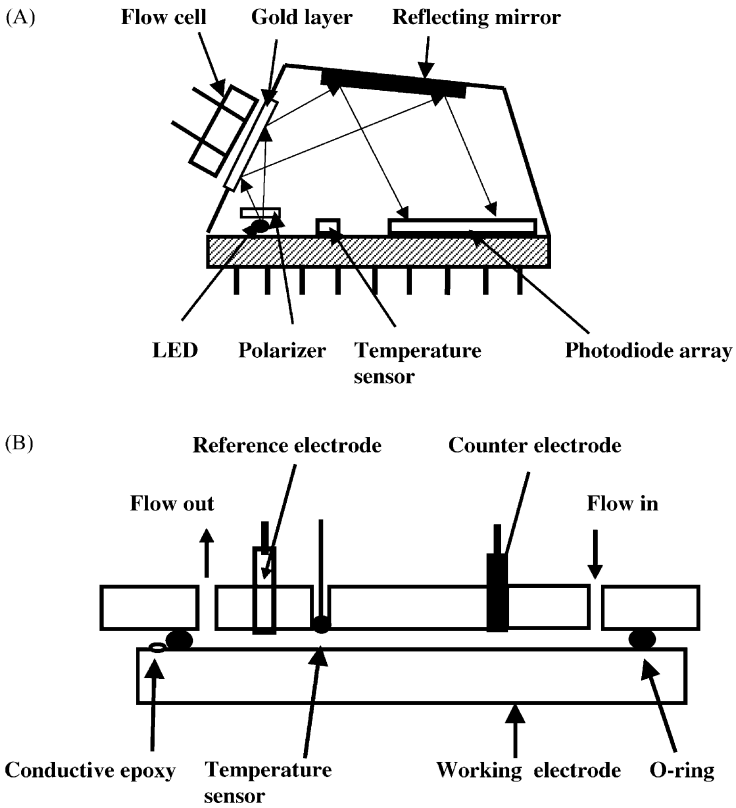

Fig. 1. (A) Schematic of the miniature Spreeta sensor. (B) Cross-sectional view of the test cell used for combined SPR/electrochemistry experiments.

molded to have optically flat surfaces. Because the system was fully encapsulated, no optical alignment is necessary. The molded epoxy is shaped in the form of the Kretschmann geometry prism to facilitate the excitation and detection of surface plasmon resonance. The surface plasmon resonance glass sensing side of the sensor was modified with 10–20 Å chromium adhesion layer evaporated onto the surface, followed by the evaporation of 500 Å of gold onto the chromium.

A small flow cell was attached to the sensor to enable the delivery of solutions across the sensing surface. In the electrochemical experiments, the gold surface of the SPR substrate also serves as the working electrode. Electrical contact with the gold surface was realized by attaching a wire via conductive silver epoxy with the contact shielded from water. Additional Ag/AgCl reference and Pt counter electrodes were introduced at the top of the flow cell to create a three-electrode configuration (Fig. 1B).

Each experiment was performed with a new Au surface. Before starting an experiment, the gold surface of the SPR substrate was thoroughly cleaned using a cotton tip, dipped in 0.1% Triton and followed by immersion in 0.12 N NaOH to remove organic residues on the Au surface. The flow cell was assembled and system was flushed first with ethanol, then with DI water, 0.1% Triton and 0.12 N NaOH solution followed by DI water again. For all experiments, the flow cell was equilibrated in running PBS buffer until a stable baseline SPR signal was obtained. All data was acquired using refractive index (RI) temperature compensation and each data point was the average of 3–5 measurements. Experiments were carried out at room temperature (20–21 °C).

Equipment for the electrochemical analysis included a CV-50 W voltammetric analyzer (Bioanalytical Systems, West Lafayette, IN). The electrochemical apparatus was controlled and data acquired using

a Dell Pentium PC. Cyclic voltammetry from 0 to 500 mV (versus Ag/AgCl electrode), at the scan rate of 20 mV/s, was used to measure the substrate-dependent current produced by the redox polymer–glucose oxidase thin films challenged with varying concentrations of glucose.

3.2. FT-IR analysis of the RP–GOX nanocomposite films

Nanocomposite thin films for FT-IR characterization studies were manufactured on gold wafers (1 in. × 1/2 in.) according to the procedure published previously [9]. In brief, the electrode surface was functionalized with a negative surface charge by exposure to 1 mM MUA (ethanol) for 20 min. The substrates were washed with ethanol and dried under N_2. The wafers were then alternately exposed to a polycationic (10 mg/ml) solution of PVP-Os-AA for ∼20 min and a polyanionic solution of GOX (10 mg/ml in PBS) for ∼20 min. In between immersions, the substrates were rinsed with 0.1 M PBS and dried under flowing N_2. FT-IR–ERS experiments were conducted using a Bio-Rad FTS-40 spectrometer equipped with a Harrick Scientific Seagull reflection accessory (Harrick Instruments Inc., Ossining, NY) and a liquid N_2-cooled, narrow-band MCT detector. Spectra were obtained using p-polarized light at an 85° angle of incidence with respect to the substrate normal. The instrument was set to a resolution of 4 cm^{-1} and 1056 scans.

4. Results and discussions

4.1. SPR analysis of the assembly of nanocomposite films

Since the pK_a of MUA is approximately 6.5 [18], a self-assembled monolayer, partially deprotonated in the neutral environment of PBS (pH ∼7.4), creates a net negative charge at the surface–solution interface. The redox polymer on the other hand possesses a net positive charge due to amine and organometallic functional groups, and therefore, it is electrostatically bound to the negatively functionalized surface. In the experiments described hereafter, a single cycle of thin film assembly is completed by the adsorption of the electronegative glucose oxidase onto the positively charged surface.

Fig. 2 shows changes in refractive index at the SPR chip surface with time for a single binding step. The rapid signal increase in the first few seconds after introduction of RP may be attributed to the change in

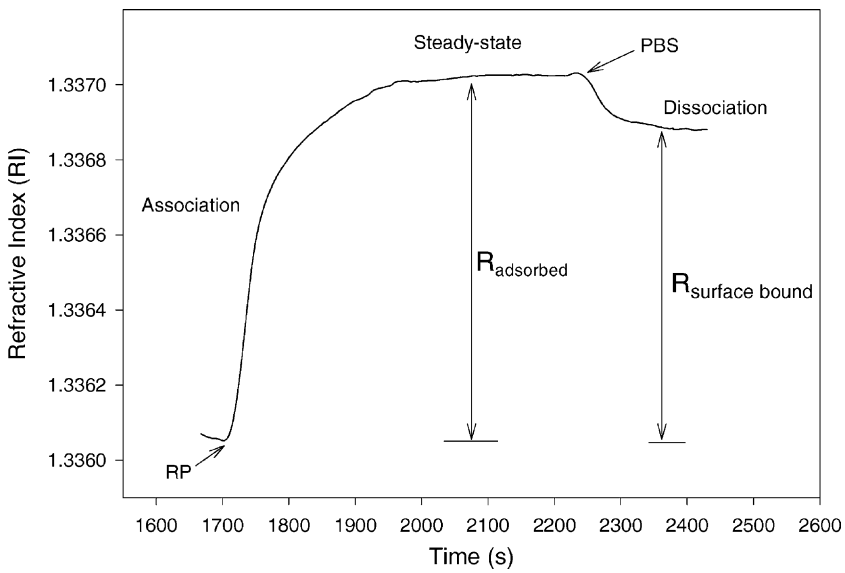

Fig. 2. Change in refractive index with time for the assembly of a single electrostatic layer of RP (10 mg/ml in PBS, flow rate 80 μl/min).

the bulk refractive index of solution [19,20]. This is followed by a gradual increase that represents the adsorption of material from solution onto the charged surface. When the surface has equilibrated, a plateau in the SPR signal is observed (see Fig. 2). At this point, the maximum concentration of polyelectrolyte (RP in the case of Fig. 2) has adsorbed onto the surface. Once a wash solution is introduced again into the flow-through cell, another sharp change (drop) in SPR response indicates change in the bulk refractive index of solution. This is followed by the desorption of the loosely bound ligand from the charged surface. Thus, a difference between initial and final RI represents the change in RI due to surface bound material.

Fig. 3 shows the change in RI for the assembly of a three RP–GOX bilayer structures on the gold surface of the chip. Initially, PBS was injected at the flow rate of 80 μl/min in order to establish a steady baseline. A high flow rate was chosen to minimize possible mass transport limitations to adsorption [21]. Following this, the surface was exposed to a solution of 1 mM MUA in absolute ethanol. The high RI (1.36192) obtained in this step of the experiment corresponds to the refractive index of ethanol. One should note instantaneous SPR signal saturation, which is indicative of very fast kinetics of thiol chemisorption on gold [22]. The surface functionalization step was followed with a washing step, when first, ethanol was circulated to wash away weakly bound MUA molecules, and then PBS was flushed through the system. As result, RI dropped to 1.33862 so that a difference of 0.00365 RI units between PBS baselines before and after introduction of MUA solution clearly points toward the presence of surface bound MUA monolayer and indicates successful functionalization of gold SPR surface. Injection of RP solution (10 mg/ml in PBS) into the flow-through system once again results in an increase of RI, however, this step may involve a slower process of electrostatic assembly, and hence, saturation of SPR signal is reached after 4.6 min. RP solution was then replaced with PBS and a new baseline was established. A change in SPR signal before and after the introduction of RP once again pointed to surface

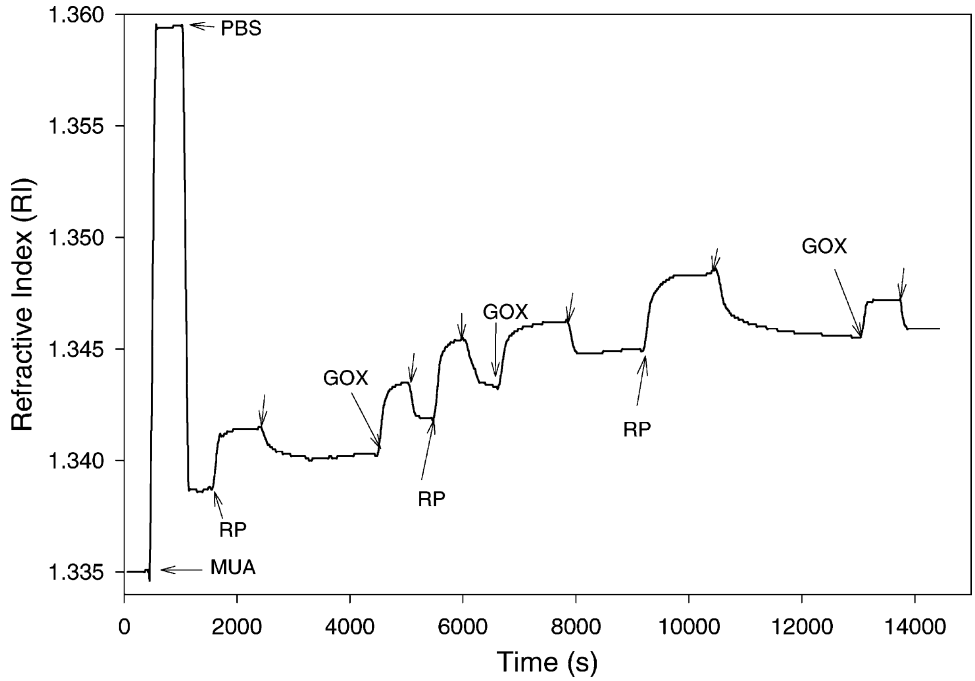

Fig. 3. SPR analysis of the assembly of the nanocomposite thin film consisting of MUA and three RP–GOX bilayers. The concentrations of RP and GOX were 10 mg/ml in PBS, flow rate 80 μl/min. Arrows indicate injections of PBS solution, needed to remove non-specifically adsorbed material.

Table 1
Change in refractive index upon the addition of each layer of the electrostatically assembled multilayered GOX/redox polymer structure ($n = 3$)

Layer	Average SPR signal in RI units ($n = 3$)	S.D. (%)
MUA	0.00350	2.9
RP-first layer	0.00137	15.2
GOX-first layer	0.00173	8.8
RP-second layer	0.00143	8.1
GOX-second layer	0.00133	8.7
RP-third layer	0.00083	6.9
GOX-third layer	0.00033	17.3

immobilization of this cationic polymer. The same procedure was repeated for GOX (10 mg/ml in PBS).

Changes in refractive index resulting from the adsorption of the various thin film components were generally reproducible from SPR chip to SPR chip. These changes are summarized in Table 1. The relatively high standard deviation seen for the first redox polymer layer is likely produced by defects in MUA monolayer resulting in variations in the amount of redox polymer adsorbed to the MUA surface. However, those variations were not translated to the first GOX layer as multivalent interactions are possible between single redox polymer and GOX macromolecules, thus insuring relative uniform adsorption of GOX despite small variations in the redox polymer layer. In addition to GOX, assembly of LOX and PYX onto the pre-adsorbed RP layer was investigated. Binding responses of 0.9×10^{-3} and 6.9×10^{-3} RIU were observed for the adsorption of LOX and PYX, respectively.

Fig. 3 and Table 1 show that the binding response for the third bilayer of GOX and RP is smaller while the standard deviation for the GOX layer is larger than in the adsorption steps for the two preceding bilayers. The increase in standard deviation and decrease in the binding response for the third bilayer of GOX and RP is likely due to the limited depth of penetration of the surface plasmon wave [23]. This hypothesis is supported by FT-IR–ERS (which has depth of penetration of several micrometers) experiments presented later in this manuscript, as well as results obtained by others [10,24], where proportional increase in the amount of enzyme with increasing number of composite layers was observed.

In order to verify, in situ, analyte-dependent activity of the glucose oxidase–redox polymer nanostructured films, the SPR test cell was modified with counter and reference electrodes while SPR sensing surface served as a working electrode (see Fig. 1B for details). Substrate calibration curves were then obtained by introducing varying concentrations of glucose into the SPR flow cell and measuring the amperometric response of the sensing films by means of the potentiostat. The sensor response was found to be linear for glucose concentrations ranging from 1 to 10 mM with sensitivity of 0.197 $\mu A/cm^2/mM$. These results compare favorably with amperometric responses observed in our previous studies of the similar sensing system [25].

SPR analysis was also employed to conduct structural stability studies of the assembled three-bilayer nanocomposite films. Assembled structures, containing RP–GOX bilayers, were stored in an aqueous environment at 4 °C and monitored with SPR for the duration of 3 weeks. No change in SPR signal was detected during the experiment, pointing to the structural integrity of the assembled film when stored in solution.

4.2. Influence of redox polymer and enzyme concentration on surface coverage

SPR spectroscopy offers an opportunity to observe, in real time, events associated with molecule–surface electrostatic interactions. In the present study, dependence of the polyelectrolyte solution concentration on the surface coverage was investigated for both RP and GOX. Adsorption of the charged molecules onto oppositely charged surface is defined by the surface charge density and the solution concentration of the adsorbing material [26]. In order to ensure maximum surface charge density, varying solution concentrations of polyelectrolyte sensor components were introduced into the flow cell of the SPR instrument. Changes in the SPR signal (in RIU) were then monitored to determine the solution concentration of polyelectrolyte which provided maximum surface coverage. Once such conditions were established, adsorption of the polyelectrolyte of interest from the solution onto the charged surface was investigated. Fig. 4 demonstrates adsorption of GOX onto the gold surface covered with MUA and the cationic RP layer.

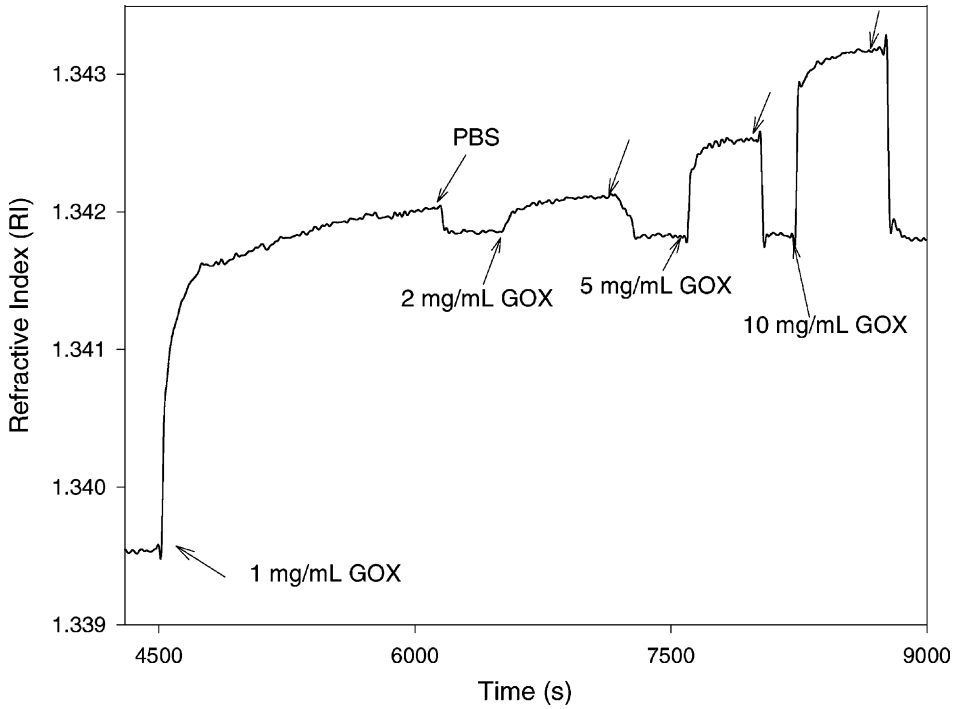

Fig. 4. Determination of the minimum GOX concentration needed for complete surface saturation. Flow rate 80 μl/min was employed. Each equilibrium state was followed by flushing with PBS. These steps are denoted by arrows.

Here, enzyme concentration of 1 mg/ml in PBS introduced at the flow rate of 80 μl/min was found to cause complete surface saturation so that consecutive challenges of the same surface with higher concentrations of the enzyme do not result in the change of $R_{\text{surfacebound}}$ SPR signal. This technique was used to ascertain minimum solution concentrations needed for complete surface saturation to occur. Detailed investigations showed that 90% of maximum SPR signal change in response to the binding of cationic polymer occurred at the RP concentration of 1 mg/ml. Similar experiments conducted for anionic GOX yielded the minimum concentration of 0.05 mg/ml. Minimizing the solution concentration of polyelectrolytes necessary for complete surface coverage is desired since both RP and enzymes are expensive.

One should note that, in principle, mass transfer limitations could obscure sensor component optimizations experiments, however, a relatively high flow rate of 80 μl/min and extensive assembly times used in these experiments should have minimized any mass transport effects.

4.2.1. Enzyme deposition and surface coverage

In the study, conducted by Stenberg et al., calibration of the SPR signal with the surface concentration of radiolabeled proteins demonstrated that shift of θ_{SPR} by 1° corresponded to deposition of 10 ng/mm^2 of protein [27]. This relationship was also found to hold true for proteins of varying molecular weights. Since SPR signal can be alternatively recorded in RI units or angle θ_{SPR}, surface concentration of GOX for each of the three deposition steps was easily found using the experimentally determined conversion factor of 7×10^{-3} RIU/°. A surface concentration of 2.4 ng/mm^2 observed in the first GOX assembly step and 1.9 ng/mm^2 for the second GOX assembly step compare favorably with values of 3.1 ng/mm^2 obtained by Hodak et al. in a QCM study of a GOX deposition onto a positively charged gold surface [13]. Similarly, surface concentrations for LOX and PYX were estimated to be 1.29 and 10.7 ng/mm^2, respectively.

Assuming the density of protein to be 1.3 g/cm^3 and a densely packed layer [2], the thickness of the first deposited enzyme layer can be approximated to be

19 Å. While this result does not represent true height of the adsorbed enzyme because surface coverage is not 100%, it may still indicate presence of a monolayer of protein on the positively charged surface. However, given known crystallographic dimensions of GOX [28], it is highly unlikely that all the adsorbed protein is GOX. This result is not unexpected. All enzyme formulations are contaminated with other proteins and protein fragments of the enzyme of interest. For example, GOX Type X-S from Sigma–Aldrich is known to be contaminated with catalase and invertase. In addition, the formulation may likely contain lytic and denatured fragments of GOX and other proteins. Thus the adsorbed protein layer may be a mixture of proteins possessing net negative charge.

A maximum surface coverage (in ng/mm^2) for the densely packed enzyme monolayer may be found using the following formula [29]:

$$P_{\text{ideal}} \sim \frac{10^{21}\, M_{\text{W}}}{\pi ab N_{\text{a}}} \tag{1}$$

where M_{W} is the molecular weight (18.6 kDa for GOX, 260 kDa for POD and 80 kDa for LOX), N_{a} the Avogadro's number and πab is an ellipsoid surface projection of the globular enzyme, with a and b being the radii of the short and long axis of the ellipse. In case of PYX and LOX, crystallographic data does not exist and the ellipsoid surface projection was simplified to πr^2 where r is a hydrodynamic radius. Taking GOX dimensions of 30 and 40 Å for a and b, respectively [28], P_{ideal} was calculated to be 8.19 ng/mm^2. In case of PYX, taking into account 50 Å hydrodynamic radius, P_{ideal} was found to be 5.5 ng/mm^2. Surface coverage was then found by means of the following relationship:

$$\text{surface coverage (\%)} = \left(\frac{P_{\text{expected}}}{P_{\text{ideal}}}\right) \times 100 \tag{2}$$

Results for the first two GOX layers, 30 and 23%, respectively are reasonable considering that maximal obtainable coverage for irreversible adsorption of protein is hypothesized as being 55% [26,30]. Such low surface coverage is thought to occur because of the steric hindrance and electrostatic repulsion between adsorbing protein molecules [26]. Another explanation may be the fact that lyophilized enzyme powders are not pure and thus the measurement techniques reports an average for all the proteins adsorbed. Thus, one could expect competitive protein adsorption onto the redox polymer surface, which may also account for a lower surface coverage for GOX.

While lack of crystallographic data for LOX does not permit one to approximate surface coverage, one could infer formation of a sub-monolayer of enzyme from a relatively weak surface coverage. On the other hand, PYX surface coverage is estimated to be 194%. This result may indicate partial denaturation or surface aggregation of the less stable PYX tetramer [31].

4.2.2. Affinity constant determination

SPR measurements with the Spreeta device were also used to determine the affinity constant between the GOX and the redox polymer layers. Surface assembly of electrostatic layers was assumed to follow a simple mechanism: $A + B \leftrightarrow AB$. The intrinsic reaction rate of the process can then be expressed by the following rate equation [19,20]:

$$\frac{\text{d}[AB]}{\text{d}t} = k_{\text{a}}[A][B] - k_{\text{d}}[AB] \tag{3}$$

where k_{a} is the association constant, k_{d} the dissociation constant, $[A]$ the concentration of sensor component in solution, $[B]$ the concentration of pre-adsorbed charged layer and $[AB]$ is the concentration of the electrostatic complex. It is more convenient to write this equation in terms of SPR response. The following terms need to be introduced: R_{max} is proportional to the maximum concentration of pre-adsorbed material ($[B]+[AB]$), R the proportional to the concentration of surface bound species $[AB]$, so that $R_{\text{max}} - R$ describes the unoccupied charged sites of the surface-bound layer. In addition, $[A]$ is assumed to be constant due to continuous supply of redox polymer solution provided by flow cell. Then, Eq. (4) may be rewritten as

$$\frac{\text{d}R}{\text{d}t} = k_{\text{a}}\, C (R_{\text{max}} - R) - k_{\text{d}} R \tag{4}$$

At steady state ($\text{d}R/\text{d}t = 0$), Eq. (4) becomes further

$$\frac{R}{C} = KR_{\text{max}} - KR \tag{5}$$

where K is the affinity constant, $k_{\text{a}}/k_{\text{d}}$.

Hence, an SPR response R can be obtained for a given concentration of sensor component by subtracting SPR signals of a baseline and steady state (see Fig. 2), so that a plot of R/C versus R will yield the

affinity constant *K*. Eq. (3) may be utilized further to obtain expressions for association and dissociation constants. However, the electrostatic assembly process investigated here poses several issues, which hinder observation of true association and dissociations events. Competitive protein adsorption, as described earlier, may obscure true association kinetics. In addition, intercalation of enzyme into the assembled layers should also influence SPR signal. Finally, despite of high flow rate, mass transfer limitations may also be encountered. Therefore, we chose to report apparent affinity or equilibrium constant, which is less susceptible to the effects described previously.

In order to ascertain apparent affinity constant, the concentration of GOX was varied from 0.05 to 10 mg/ml while RP concentration was held constant at 10 mg/ml to obtain changes in RI similar to those shown in Fig. 5. A new SPR chip was used for each GOX concentration. Using Eq. (5), binding constant *K* for deposition of first layer of GOX was found to be of $8 \times 10^7\,M^{-1}$. This results clearly demonstrates the high affinity of the anionic enzyme for the cationic RP, a result of the multiple electrostatic contacts between the two macromolecules. Since surface concentrations for the first and the second enzyme layers were found to be similar, affinity constants for the two layers are presumed to be the same.

4.3. FT-IR analysis of the RP–GOX nanocomposite films

FT-IR–ERS spectra collected from thin films composed of the varying number of layers are shown in Fig. 6. Thin films containing one (three total layers), two (five total layers) and three (seven layers total) nanocomposite layers were examined, with the control being a film comprised of MUA–redox polymer only. The particular focus of this study was placed on verifying incorporation of glucose oxidase into the layer-by-layer structure, hence, regions associated with polypeptide bonds were examined. The spectra from these regions, 3400–3200 cm^{-1} and 1800–1400 cm^{-1}, are shown in Fig. 6a and b, respectively. Broad absorbance peak around 3310 cm^{-1} observed in Fig. 6a is assigned to N–H stretching vibrations ($\nu_{N–H}$). This absorbance band is not present in the control sample containing MUA–RP and has been attributed to the presence of the enzyme previously [32]. Amides 1 (1668 cm^{-1}) and 2 (1543 cm^{-1}) regions shown in Fig. 6b are characteristic of the

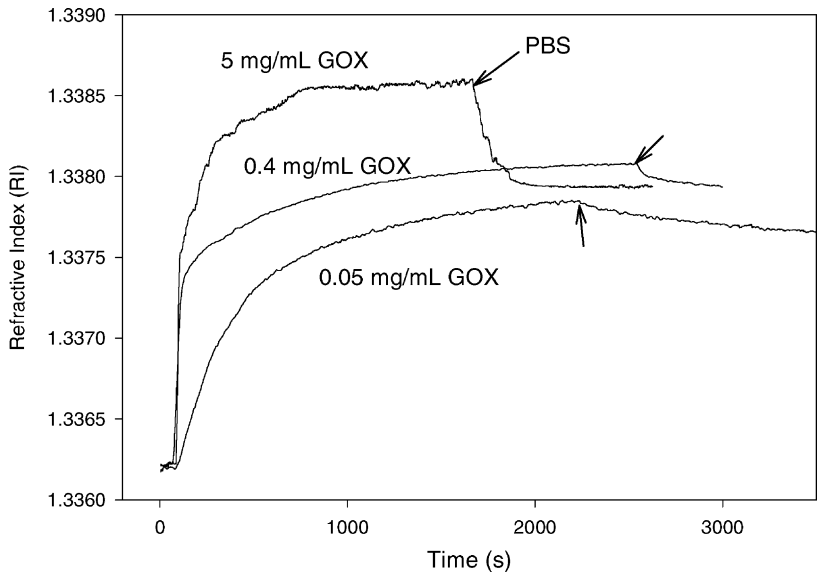

Fig. 5. Affinity constant determination for the binding of GOX (flow rate 80 μl/min) with surface-bound RP layer. Arrows denote injections of PBS wash solution.

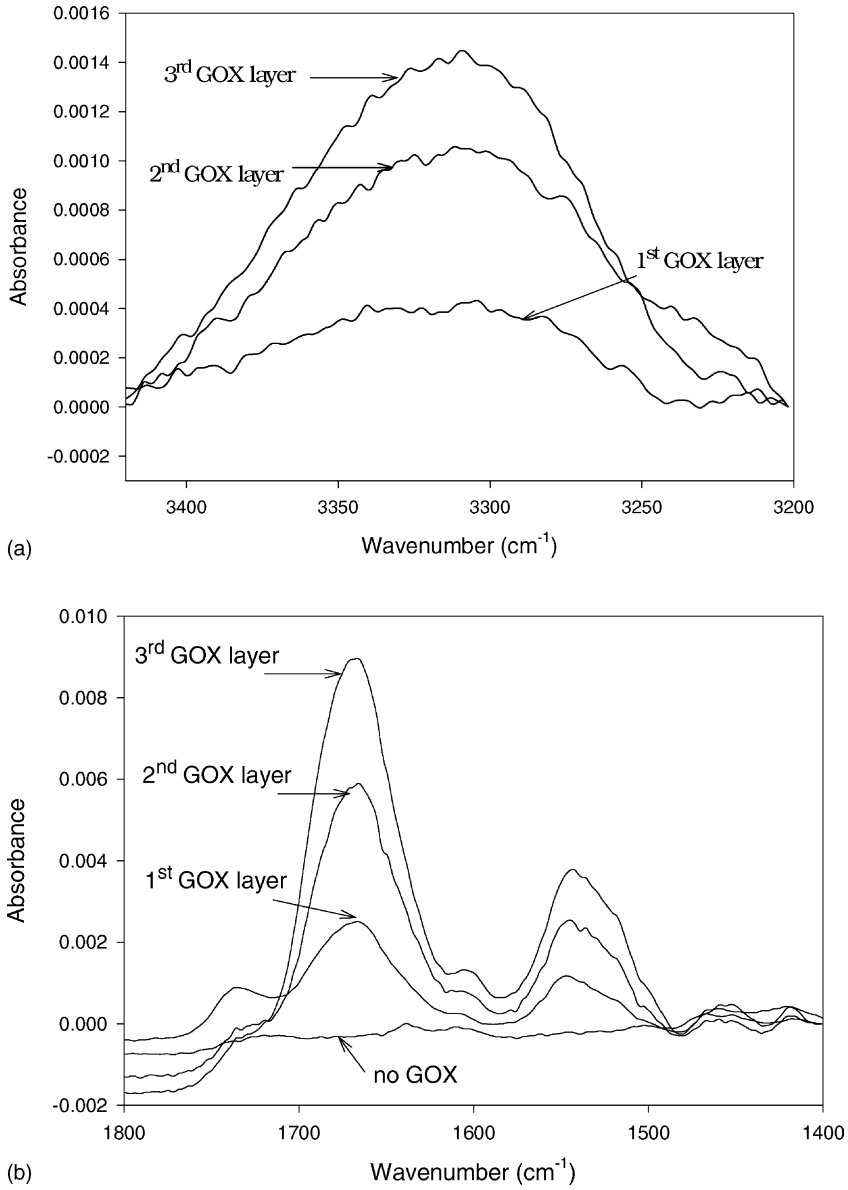

Fig. 6. (a) Amine stretching region of FT-IR–ERS spectrum collected from a thin film consisting of three RP–GOX bilayers. (b) Amides 1 and 2 regions of the FT-IR–ERS spectrum collected from the same nanocomposite film.

protein polypeptide bonding. Specifically, the amide 1 absorbance band is normally attributed to stretching vibrations of the peptide carbonyl groups while the amide 2 absorbance region occurs due to N–H bending and C–N stretching of the polypeptide bonds [33]. Positions of amides 1 and 2 peaks compare well with other studies where GOX was incorporated into thin films [34] and suggest a secondary structure of α-helices and β-sheets [33]. As seen from Fig. 7, absorbance in the ν_{N-H}, amides 1 and 2 regions increase as number of enzyme layers increases. No peak shifting occurs during the assembly, which should point toward depth uniformity of the film [35]. Fig. 7 also demonstrates linear dependence of absorbance

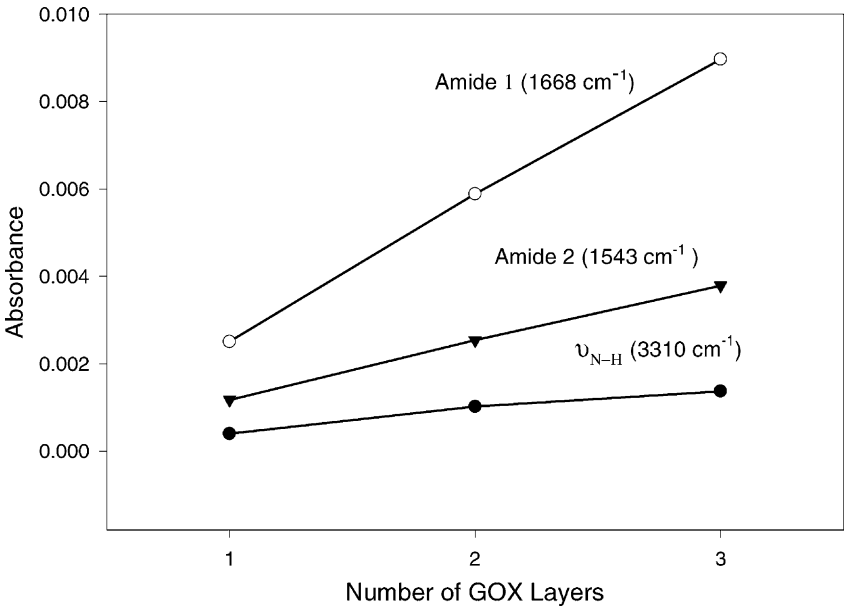

Fig. 7. Plot representing absorbance in the amine stretching and amides 1 and 2 regions as a function of number of layers.

on the number of layers for amides 1and 2 and ν_{N-H} regions.

To assess whether structural changes occur in entrapped GOX, FT-IR–ERS spectra of the thin films containing one GOX layer were obtained immediately upon assembly and after 3 weeks of dry storage at 4 °C. No changes in the positions of the amides 1 and 2 bands were observed, indicating that enzyme may not have undergone changes in secondary structure. Previous studies have connected loss of enzymatic activity to changes in secondary structure represented by the shifts in the positions of these peaks [34]. Thus loss of sensor activity with time is likely not due to the loss of enzyme from the sensor surface or due to the denaturation of the enzyme, but may be due to the inactivation of the FAD redox center of the enzyme. This mechanism of inactivation would lead to an inactive sensor, but little or no changes in film structure as we have observed.

The use of FT-IR–ERS for the analysis of the redox polymer in the nanostructured films is made difficult by the appearance of the absorbance peaks associated with the polymer in the amides 1 and 2 regions. For example, the peak around 1640 cm^{-1} present in the control sample and attributed to primary amines of the redox polymer is overlapped by the very strongly absorbing amide 1 band. Another peak at 1600 cm^{-1}, assigned to the ring vibration of the pyridine group of the Os-based redox polymer [36], may contribute to the shoulder of the amide 1 region. While redox polymer is difficult to detect with this method, its adsorption was conclusively demonstrated by SPR. In addition, presence of the cationic polymer is necessary for the uniform assembly of the anionic enzyme observed by FT-IR experiments to occur.

5. Conclusions

In conclusion, we have used SPR sensing and FT-IR–ERS to investigate the layer-by-layer assembly of nanocomposite redox polymer/oxidoreductase films on gold surfaces. Such investigation is an important step toward better understanding of assembly processes and properties of the assembled thin films. In this manuscript, the surface coverage of the deposited GOX, LOX and POD enzymes were estimated by means of SPR spectroscopy. In addition, the affinity constant for GOX–RP binding was found. FT-IR–ERS was also utilized to verify incorporation

of the GOX into the nanostructured films and investigate changes in enzyme secondary structure with time. SPR instrument was also coupled to a potentiostat to enable real-time monitoring of RP–GOX nanocomposite film assembly and verification of electron transfer between the enzyme and redox polymer.

Acknowledgements

The authors would like to thank Texas Instruments Incorporated for providing the TISPR-1 sensor and Experimenter's Kit. Help and comments provided by Dr. Clem Furlong, Dr. Dwight Bartholomew, Dr. Anita Strong, Dr. John Quinn and Dr. Li Sun are greatly appreciated. We would also like to thank Dr. Richard Crooks from the Department of Chemistry at Texas A&M University and his group members for the use of FT-IR–ERS instrument. Financial support for JWR was provided in part by the Department of Energy Office of National Security and Nonproliferation, and by US Army Medical Research and Materiel Command. MVP, AS, and AR thank the National Science Foundation (CTS-9875372) and the US Department of the Army and the National Medical Technology Testbed Inc. (DAMD17-97-2-7016) for funding. MVP acknowledges the support of the Alfred P. Sloan Foundation through a research fellowship. "This work does not necessarily reflect the position or the policy of the government or NMTB, and that no official endorsement should be inferred." This work was partially funded by the US Department of the Army and the National Medical Technology Testbed Inc. (DAMD17-97-2-7016). "This work does not necessarily reflect the position or the policy of the government or NMTB, and that no official endorsement should be inferred."

References

[1] G. Decher, Science 227 (1997) 1232–1237.
[2] Y. Lvov, K. Ariga, I. Ichinose, T. Kunitake, J. Am. Chem. Soc. 117 (1995) 6117–6123.
[3] P.T. Hammond, G.M. Whitesides, Macromolecules 28 (1995) 7569–7571.
[4] S.L. Clark, P.T. Hammond, Adv. Mater. 10 (1998) 1515–1519.
[5] A. Heller, Accounts Chem. Res. 23 (1990) 129–134.
[6] M.V. Pishko, I. Katakis, S.-E. Lindquist, L. Ye, B.A. Gregg, A. Heller, Angew. Chem. Int. Ed. 29 (1990) 82.
[7] M.V. Pishko, A.C. Michael, A. Heller, Anal. Chem. 63 (1991) 2268–2272.
[8] S.-F. Hou, H.-Q. Fang, H.-Y. Chen, Anal. Lett. 30 (1997) 1631–1641.
[9] K. Sirkar, A. Revzin, M.V. Pishko, Anal. Chem. 72 (2000) 2930–2936.
[10] E.J. Calvo, F. Battaglini, C. Danilowicz, A. Wolosiuk, M. Otero, Faraday Dis. 116 (2000) 47–65.
[11] A. Narvaez, G. Suarez, I.C. Popescu, I. Katakis, E. Dominguez, Biosens. Bioelectron. 15 (2000) 43–52.
[12] E.J. Calvo, R. Etchenique, L. Pietrasanta, A. Wolosiuk, C. Danilowicz, Anal. Chem. 73 (2001) 1161–1168.
[13] J. Hodak, R. Etchenique, E.J. Calvo, K. Singhal, P.N. Bartlett, Langmuir 13 (1997) 2708–2716.
[14] D. Laurent, J.B. Schlenoff, Langmuir 13 (1997) 1552–1557.
[15] E.M. Kober, J.V. Caspar, B.P. Sullivan, T.J. Meyer, Inorg. Chem. 27 (1988) 4587–4598.
[16] J. Melendez, R. Carr, D.U. Bartholomew, K. Kukanskis, J. Elkind, S. Yee, C. Furlong, R. Woodbury, Sens. Actuators B 35/36 (1996) 212–216.
[17] J.L. Elkind, D.I. Stimpson, A.A. Strong, D.U. Bartholomew, J.L. Melendez, Sens. Actuators B 54 (1999) 182–190.
[18] C.E. Jordan, R.M. Corn, Anal. Chem. 69 (1997) 1449–1456.
[19] J. Lahiri, L. Isaacs, J. Tien, G.M. Whitesides, Anal. Chem. 71 (1999) 777–790.
[20] R.J. Green, R.A. Frazier, K.M. Shakesheff, M.C. Davies, C.J. Roberts, S.B. Tendler, Biomaterials 21 (2000) 1823–1835.
[21] D.J. Myszka, Mol. Recognition 12 (1999) 279–284.
[22] K.A. Peterlinz, R. Geordiadis, Langmuir 12 (1996) 4731–4770.
[23] L.S. Jung, C.T. Campbell, T.M. Chinowsky, M.N. Mar, S.S. Yee, Langmuir 14 (1998) 5636–5648.
[24] F. Caruso, K. Nikura, D.N. Furlong, Y. Okahata, Langmuir 13 (1997) 3427–3433.
[25] A. Revzin, K. Sirkar, A.L. Simonian, M.V. Pishko, Sens. Actuators B 81 (2002) 359–368.
[26] Y. Yuan, M.R. Oberholzer, A.M. Lenhoff, Coll. Surf. 165 (2000) 125–141.
[27] E. Stenberg, B. Persson, H. Roos, C. Urbaniczky, J. Coll. Interface Sci. 143 (1991) 513–526.
[28] H.J. Hecht, D. Schomburg, H. Kalisz, R.D. Schmid, Biosens. Bioelectron. 8 (1993) 197–203.
[29] J. Lahiri, L. Isaacs, B. Grzybowski, J.D. Carbeck, G.M. Whitesides, Langmuir 15 (1999) 7186–7198.
[30] X. Jin, N.-H. Wang, G. Tarjus, J. Talbot, J. Phys. Chem. 97 (1993) 4256–4258.
[31] N. Gajovic, K. Habermuller, A. Warsinke, W. Schuhmann, F. Scheller, Electroanalysis 11 (1999) 1377–1383.
[32] F. Caruso, D.N. Furlong, K. Ariga, I. Izumi, T. Kunitake, Langmuir 14 (1998) 4559–4565.
[33] D.M. Byler, H. Susi, Biopolymers 25 (1986) 469–487.
[34] J.G. Franchina, W.M. Lackowski, D.L. Dermody, R.M. Crooks, D.E. Bergbreiter, K. Sirkar, R.J. Russell, M.V. Pishko, Anal. Chem. 71 (1999) 3133–3139.
[35] Y. Cheng, R.M. Corn, J. Phys. Chem. B 103 (1999) 8726–8731.
[36] T. Lian, E. Hao, Chem. Mater. 12 (2000) 3392–3396.